Novel terahertz metamaterial absorber with diamond-shaping split ring resonators for dual-purpose refractive index sensing

P. MUKHERJEE[1], S. MISHRA[2], S. PAHADSINGH[2], B. APPASANI[2,*], N. BIZON[3,4,5]
[1]*Department of Electrical and Computer Engineering, University of Wisconsin-Madison, USA*
[2]*School of Electronics Engineering, Kalinga Institute of Industrial Technology, Bhubaneswar 751024, India*
[3]*Piteşti University Centre, The National University of Science and Technology POLITEHNICA Bucharest, 110040 Pitesti, Romania*
[4]*ICSI Energy, National Research and Development Institute for Cryogenic and Isotopic Technologies, 240050 Ramnicu Valcea, Romania;*
[5]*Doctoral School, The National University of Science and Technology POLITEHNICA Bucharest, 110040 Pitesti, Romania*

The paper proposes a novel design for a metamaterial absorber comprised of eight concentric diamond-shaped split ring resonators (SRR), with splits and gaps introduced to optimize the performance. The sensor is set to operate at the terahertz frequency range to prevent any disturbance in the sensing mechanism. At resonance, a distinct and near-perfect absorption rate of 99.83% is obtained with an FWHM of 0.05 THz. A step-by-step methodology for finding the optimum design is discussed and analyzed through parametric optimization. The paper aims to utilize the design for refractive index sensing applications for biomedical and gas sensing applications. Sensitivities of 1.3 THz/RIU and 1.8 THz/RIU are obtained for bio-medical and gas detection, respectively. Thus, the sensor achieves dual-purpose refractive index sensing with high absorption in biomedical applications like cancer detection and the detection of gases.

(Received October 4, 2023; accepted October 7, 2024)

Keywords: Metamaterial absorber, Refractive index sensing, Split-ring resonators, Bio-medical, Gas detection

1. Introduction

In recent literature, the use of the absorption mechanism has come to be a helpful element in healthcare applications like the protection of the human body from harmful EM radiation. Absorbing electromagnetic waves helps in electromagnetic shielding [1, 2]. For this reason, it acts as a promising technology in the healthcare industry through its implementation in wearable devices and biosensing. Furthermore, at higher frequencies like the terahertz and the infrared, the radiation is non-ionizing and does not interfere with the sensing and imaging processes. Various metamaterial absorbers in the terahertz frequencies have been designed for single-band, as well as dual [3,4] and multi-band applications [5,6]. Metamaterial-based absorbers are a noteworthy method to facilitate the mechanism.

Metamaterials are plasmonic nanostructures consisting of unit cells of subwavelength units arranged periodically. A typical metamaterial absorber (MA) structure comprises a dielectric layer sandwiched between the top layer and the ground plane. The top layer is a frequency-selective surface (FSS) comprising resonators. The design used to structure the resonators, the dielectric height, the unit cell's dimensions, and the materials used determine the performance of the MA. The top and bottom layers are made up of low-loss and highly reflective metals like gold and silver. Low-loss, thermally resistant, and mechanically flexible high-dielectric materials like gallium arsenide (GaAs) are preferred for the substrate. Additionally, unit cell dimensions are preferable to be in the micrometer range to prevent Ohmic losses [7].

Sensing methods are broadly classified as label-based and label-free sensing [8]. While some samples, like organic analytes, are detected using labels like biotin based on features like fluorescence, other methods do not rely on such labels and instead perform the process of detecting based on inherent features like material, electrical, and optical properties. RI sensing is a type of such label-free sensing where the RI of the sample is used for detection. This type of sensing method is hassle-free compared to label-based sensing, can be performed in bulk, is cost-effective, and is time-efficient.

Label-free sensing based on optical properties like RI can be designed by using photonic and plasmonic devices. We use MA as the plasmonic nanostructure. An-other popular method is the use of photonic crystals. Surface plasmon resonance (SPR) is employed as the working mechanism in both MA-based and photonic crystal-based RI sensors. Literature has used different types of photonic crystals of one and two dimensions like photonic crystal fibres (PCF) [9], photonic crystal nanobeams (PCN) [10], and photonic crystal cavities [11].

To date, no work on a multi-purpose RI sensor is useful in various applications. Those covering a large refractive index range have poor linearity and low sensitivity. A high sensitivity gas sensor based on THz metamaterials was proposed in [12], but this cannot be used for bio-medical

applications. A dual-purpose sensor for RI sensing and biosensing was proposed in [13]. Mukherjee et al. [14] proposed a TMA for early cancer diagnosis yielding a sensitivity of 1.57 THz/RIU and a high figure of merit of 157.1 /RIU. In another work [15] for cancer diagnosis, a high sensitivity of 3.923 THz/RIU and FOM of 6.111 was obtained. A high sensitivity of 2.558 THz/RIU was obtained for gas detection applications in [16], while a multi-layered graphene-based metamaterial absorber for biosensing in the diagnostic applications of malaria infection [17] yielded a high sensitivity of 2.538 THz/RIU and an average Q-factor of 23.4.

The paper aims to design a refractive index (RI) sensor based on a metamaterial absorber for detecting both gases and biomedical systems, like cancer diagnosis and the detection of liquids. The sensor is set to operate at the terahertz frequency range to prevent any disturbance in the sensing mechanism.

2. Experimental

The metamaterial structure comprises a layer of gallium arsenide (GaAs, ε_r = 12.94, loss tangent, tanδ = 0.006) as the substrate sandwiched between two layers of gold. The height of substrate is t_s = 6 μm. The bottom layer is a continuous ground plane that prevents wave transmission through the absorber. Then, the transmission coefficient, T = 0, thus increasing the absorption in the structure. Mathematically, the absorption is given by:

$$A = 1 - R - T = 1 - |S_{11}|^2 - |S_{12}|^2 \quad (1)$$

where, R is the reflection coefficient. Hence, a low value of R, i.e., S_{11} parameter is necessary to increase the absorption rate. The top metal layer consists of a total of eight concentric diamond-shaped SRRs, as shown in Fig. 1. The SRRs are evenly spaced with a gap of $g = 5\ \mu m$, with varying radii ranging from $5\ \mu m$ for the innermost SRR to $40\ \mu m$ for the outermost SRR, and the width of each SRR is 1 μm. The resonators are arranged such that the resonators have a split along the vertical of width $s = 1\ \mu m$ alternatively on opposite sides. The height of the gold metal is t_m = 0.2 μm, and the complete structure has the unit cell dimension u = 100 μm.

In obtaining this design, we first started with concentric circles and squares with varying diameters. Thereafter, slits (pertaining to the parameter 's' in the proposed design) were introduced to reach the optimum performance. We observed that better performance was achieved for square-shaped resonators. Rotating the squares 45° to yield the diamond shapes resulted in better performance. To further attain the optimum values of each parameter, a parametric sweep was performed. Table 1 lists the parameters of the design and their values.

Another aspect that impacted the choice of the design was the requirement of the absorber to be dual-purpose, i.e., it should be highly performative in both the frequency ranges of 1.35 – 1.4 and 1.0 – 1.1. Hence, the parametric sweep was performed such that optimum performance was obtained for both of the frequency ranges.

Table 1. Design parameters

Parameter	Symbol	Value (in μm)
Unit cell dimension	u	100
Height of substrate	t_s	6
Height of metal	t_m	0.2
Distance between radii	g	5
Width of split	s	1
Radius of outermost SRR	a	40
Radius of innermost SRR	d	5

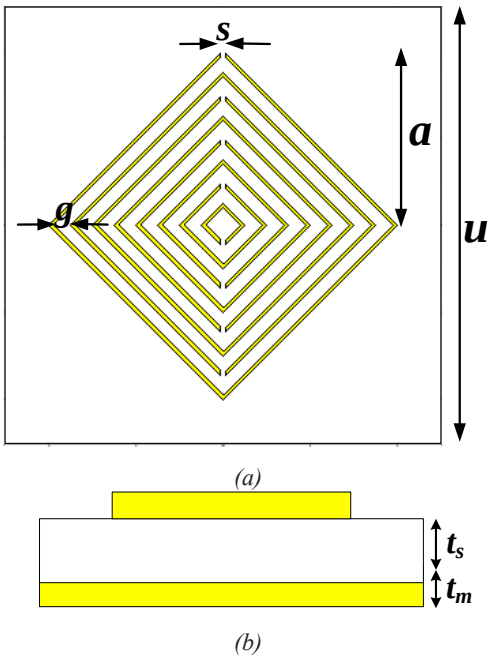

Fig. 1. Metamaterial absorber structure in (a) front, and (b) side views (color online)

3. Results and discussion

The designed MA yields an absorption rate of 99.83 % at resonant frequency, 2.7215 THz derived as per equation (1), shown in Fig. 2. A narrow width of the peak is also ensured by the low value of 0.05 THz for the full-width half-maxima (FWHM). The quality factor is obtained to be a moderate value of 54.43, as given by

$$Q = f_0/FWHM \quad (2)$$

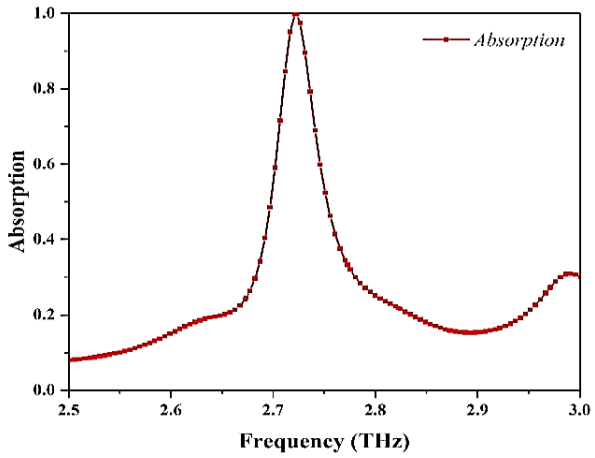

Fig. 2. Absorption rate obtained at 2.7215 THz for the designed MA (color online)

The absorption mechanism can be better understood from the impedance plot and the permittivity and permeability plot shown in Fig 3. From the Fig 3 (a), it can be observed that at resonance frequency, the imaginary part of impedance is almost zero and the real part is 400Ω, approximately equal to that of free space (377Ω). Thus, impedance matching is achieved resulting is negligible reflection. Furthermore, from Fig 3 (b), it can be observed that the real part of permittivity is negative, while that of permeability is positive, indicative epsilon negative material (ENG). This behavior causes surface plasmon resonance, which can be corroborated by the surface current distribution at the resonant frequency shown in Fig. 4.

It can be observed that the surface current moves in oscillating patterns creating hotspots at the edges of the unit cell and the thin edges of the radii. The presence of the splits makes the distribution concentrate around the edges of the resonators. The phenomenon occurs due to magnetic behavior enabled by the localized surface plasmon polaritons (LSPPs) at the metal-dielectric interface. At resonance, these get excited and, through magnetic coupling, lead to distinct narrow peaks in the absorption spectrum.

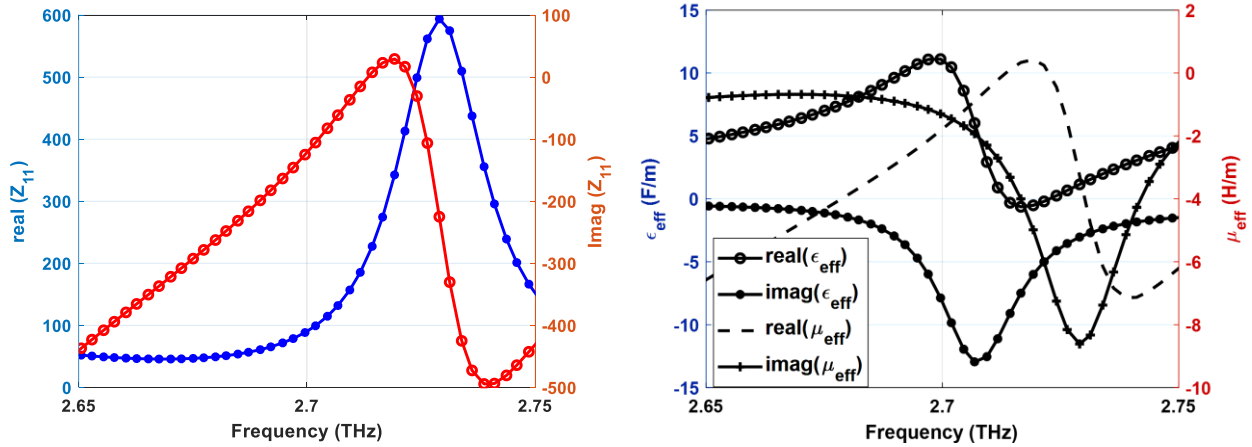

Fig. 3. Plot of (a) impedance, and (b) permittivity and permeability (color online)

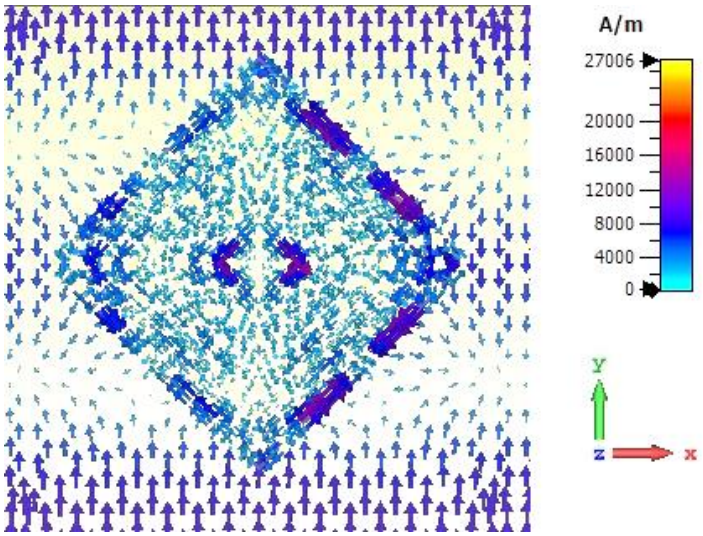

Fig. 4. Surface current distribution at resonant frequency (color online)

To arrive at an optimal design using the basic composite structures of SRRs, we first compared the results for five different shapes, vis-à-vis, circle, square, diamond, hexagon, and octagon. The fundamental design is that the resonators are grouped into four pairs where the outer radii of each pair are 10 μm, 20 μm, 30 μm, and 40 μm, respectively. The inner resonators of each pair are placed at g = 2 μm from its corresponding outer radii. The width of the split is also taken to be s = 2 μm. As shown in Fig. 5, a composite structure of diamond shaped SRRs has a maximum absorption rate of 99.4%. Therefore, we select the diamond shape and perform a parametric sweep for g over five values and s over four values to find the best results. From Fig. 6, it can thus be observed that the best results are obtained for values g = 5 μm and s = 1 μm.

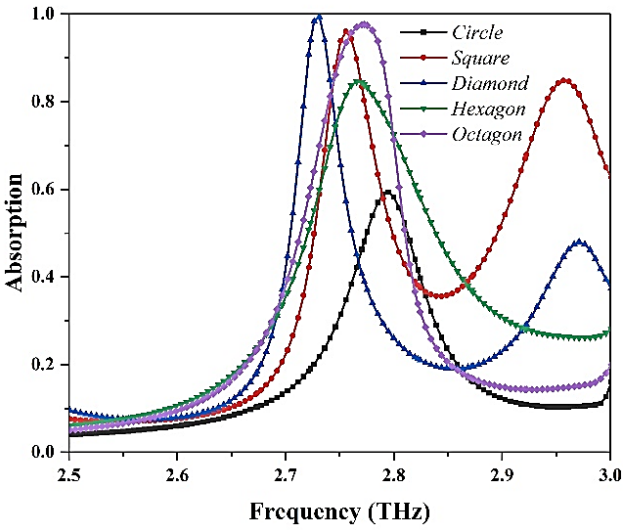

Fig. 5. Comparison of composite structures of SRRs to find the optimum design structure (color online)

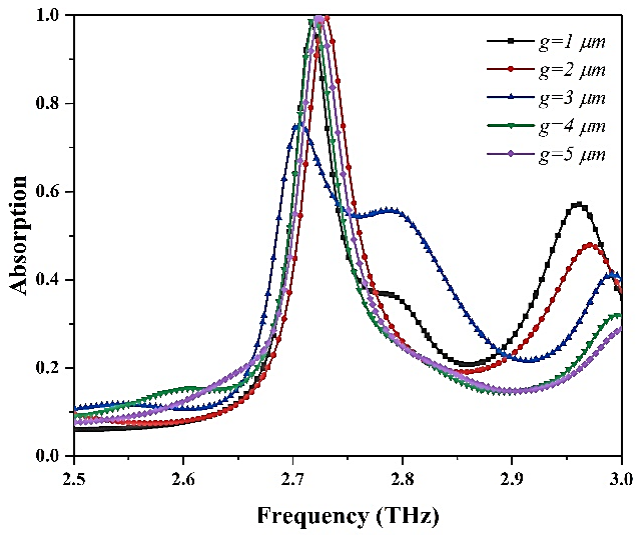

(a)

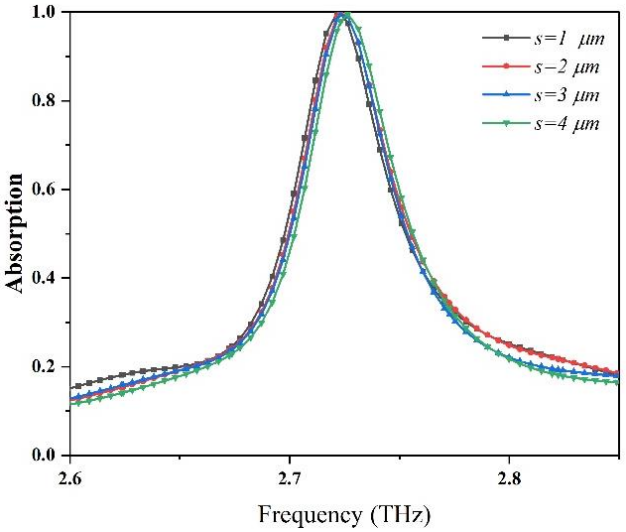

(b)

Fig. 6. Parametric sweep performed for (a) gap between radii, g, and (b) width of split s, to determine optimum values of the parameters (color online)

To further justify the processed design, we perform parametric sweep for the unit cell dimension u and height of substrate t_s over 3 consecutive values. Fig. 7 justifies that the obtained design yields a high absorption rate for the chosen set of parameter values. In Fig. 6(a), the absorption rates for all three values of u are high, and for u = 99 μm and 100 μm, the rates differ only by 0.03%. However, at u =100 μm, the optimum result is obtained by performing a parametric sweep for the height of the substrate. The peak at t_s = 5 μm is low; for t_s = 7 μm, no distinct peak is observed due to destructive interference.

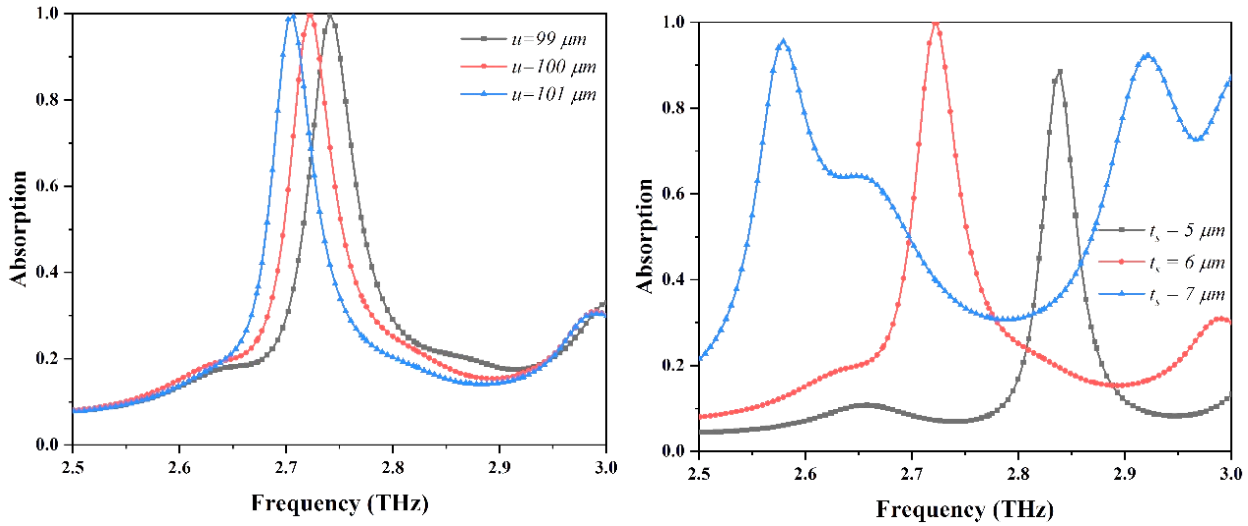

(a) (b)

Fig. 7. Parametric sweep performed for (a) unit cell dimension, u, and (b) height of substrate, t_s to justify the values of the parameters (color online)

An MA can be used in biomedical sensing applications by observing and analysing the absorption spectrum for the refractive index of a given sample. The typical refractive index range for biomedical samples ranges from 1.35 – 1.4. Sensitivity is given the ratio of the change in resonant frequency to that of the refractive index of the medium, as given in equation (3).

$$S = \Delta f / \Delta n \tag{3}$$

It is thus the slope of the frequency versus refractive index graph and can be written as a negatively sloped linear equation. The figure of merit (FOM) is another metric of measurement to understand the sensor's performance and is defined as the ratio of the sensitivity to the FWHM, given in equation (4).

$$FOM = S/FWHM \tag{4}$$

Through this MA design, we aim to sense and detect malicious cells and gases by measuring the sensitivity and figure of merit for each refractive index range.

Table 2 enlists some examples of biomedical samples that can be sensed according to their RI.

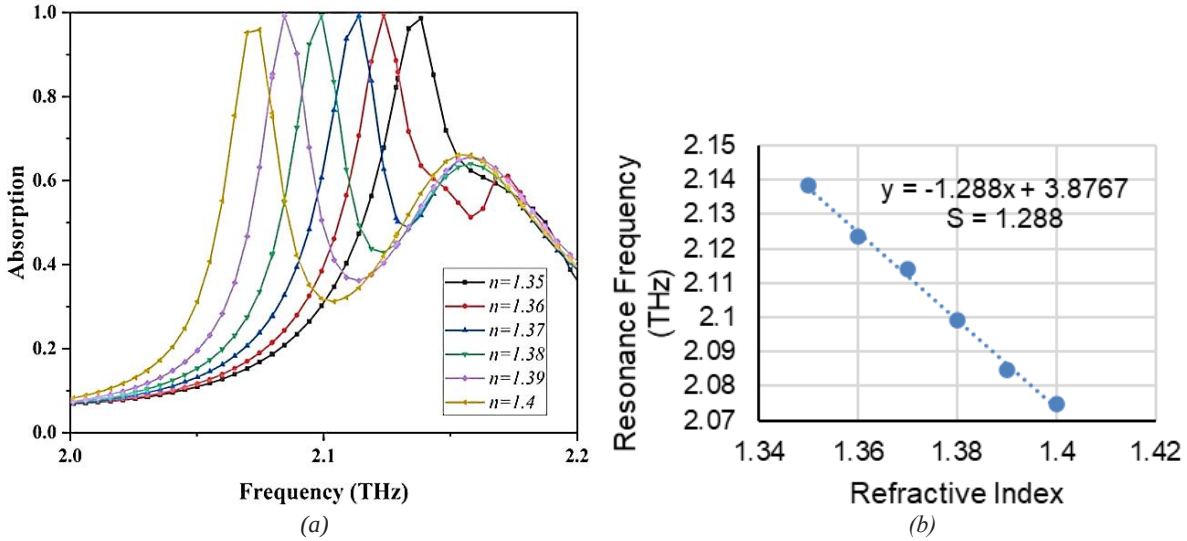

(a) (b)

Fig. 8. (a) Absorption spectrum for different refractive indices, and (b) sensitivity, for biomedical refractive index range (color online)

Table 2. Refractive indices of various biomedical systems

Biomedical systems/fluids	Refractive Index
Cancerous cells	1.35 – 1.39
Ethyl alcohol	1.36
Acetone	1.36
Heptane	1.37

Gases have refractive indices in the broad range of 1 – 1.1.

Thus, we propose a multi-functional refractive index sensor that can be used for biomedical and gas detection. Such designs can potentially be further optimized by multiple layers, especially using graphene as in [17,18], and can have multiple applications like in antennae communications due to their high absorption and polarization-insensitivity.

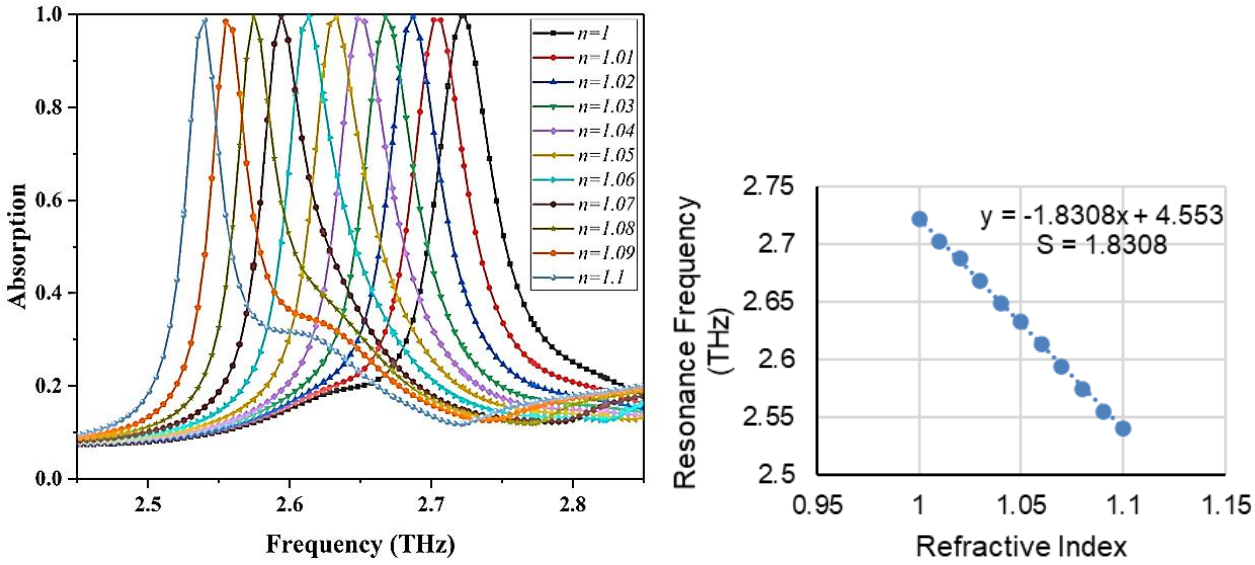

(a) *(b)*

Fig. 9. (a) Absorption spectrum for different refractive indices, and (b) sensitivity, for refractive index range of gases (color online)

Table 3. Comparison of performance of the sensor

Ref.	RI (*n*) Range	Absorption rate (%)	FOM	Sensitivity (THz/RIU)	Dual Purpose ?
[12]	1.0 – 1.1	99.3	-	3.59	No
[19]	1.0 – 1.9	99.8	6.015	0.187	Yes
[20]	1.34 – 1.39	99.4	25	1.5	No
[21]	1.35 – 1.4	99.75	-	0.851	No
[22]	1.3 – 1.39	99	2.94	0.3	No
[23]	1.0 – 1.05	99.65	106	2.12	No
[24]	1.0 – 2.0	-	-	0.061	Yes
[25]	1.0 – 1.05	99.9	~301	1.45	No
[26]	1.0 – 1.4	-	-	0.343	Yes
[27]	1.0 – 1.8	98.7	-	0.0915	Yes
This paper	1.35 – 1.4; 1.0 – 1.1	99.8	26; 36	1.3; 1.8	Yes

Table 3 provides a comparison chart of the results of the proposed sensor with other literature to assess the novelty of the same. While most of the papers referred in the table have near-perfect absorption, only [19], [24], [26], and [27] are dual-purpose in both kinds of sensing applications as proposed in this paper. In addition, our paper observes the largest sensitivities in both applications

4. Conclusion

The paper proposes a refractive index sensor based on a metamaterial absorber operating at the terahertz frequency range. It is a label-free sensing process based on surface plasmon resonance. The sensor is designed to be dual-purpose, i.e., it can be implemented in both gas detection and biosensing applications.

The report discusses the history, background theory, and working mechanism in-volved in metamaterials and metamaterial absorbers. It also explores the RI sensing mechanism and various ways it is carried out in literature. It explores the absorption process, surface current distribution and analyses the sensor's performance for both types of applications. The design is justified through parametric justification and the design methodology is explained. Finally, the sensor's performance is measured using parameter sensitivity and FOM. This is done by analyzing the absorption spectrum for two sets of refractive indices, one for each application.

The novelty of this work lies in its dual-purpose approach and near-perfect absorption of 99.8% obtained. The TMA is fit for refractive index sensing application and is aimed for sensing in both the biomedical and gas detection refractive index ranges. It is a novel design comprising four pairs of diamond shaped SRRs. Its unique shape was obtained by parametrically optimizing and analyzing similar composite structures, finally obtaining

optimum results for the proposed structure. The parameters of parameters like unit cell dimension and substrate height for the structure have also been justified by performing a parametric sweep across consecutive values. The design, therefore, yields high absorption values with a narrow FWHM of 0.05 THz. For biomedical applications, the sensitivity obtained is 1.3 THz/RIU, and that of gas detection is 1.83 THz/RIU.

Acknowledgements

The research was partially supported by the National Plan of R&D, Project PN 23 15 01 01, Contract No. 20N/2023 and by a grant of the European Regional Development Fund, within the Competitiveness Operational Program, in the frame of the project "Increasing the research capacity of ICSI Râmnicu Vâlcea through the development of a CLOUD infrastructure connected to global information resources, 4C-ICSI", SMIS 125119, project no. 345/2021.

Conflict of interest

The authors declare no conflicts of interest for this paper.

References

[1] D. Schurig, Science **314**, 977 (2006).
[2] Y. Yang, C. Song, Materials & Design **222**, 111079 (2022).
[3] Y. I. Abdulkarim, O. Altintas, A. S. Karim, H. N. Awl, F. F. Muhammadsharif, F. O. Alkurt, M. Bakir, B. Appasani, M. Karaaslan, J. Dong, ACS Omega **7**(42), 38094 (2022).
[4] M. Janneh, A. De Marcellis, E. Palange, A. T. Tenggara, B. Byun, Optics Communications **416**, 152 (2018).
[5] Y. I. Abdulkarim, M. Xiao, H. N. Awl, F. F. Muhammadsharif, T. Lang, S. Saeed, F. Alkurt, M. Bakir, M. Karaaslan, J. Dong, Optical Materials Express **12**(1), 338 (2022).
[6] P. Zamzam, P. Rezaei, S. A. Khatami, Physica E: Low-dimensional Systems and Nanostructures **128**, 114621 (2021).
[7] R. Rahad, A. K. M. Rakib, M. A. Haque, S. S. Sharar, R. H. Sagor, Results in Physics **49**, 106478 (2023).
[8] V. R. Samuel, K. J. Rao. Biosensors and Bioelectronics: X **11**, 100216 (2022).
[9] H. Liang, T. Shen, Y. A. Feng, Sensors **21**, 71 (2020).
[10] B. Duan, S. Liu, X. Liu, Results in Physics **47**, 106304 (2023).
[11] F. Peng, Z. Wang, G. Yuan, IEEE Photonics Journal **10**, 1 (2018).
[12] B. Appasani, A. Srinivasulu, C. A. Ravariu, Defence Technology **22**, 69 (2023).
[13] S. Yan, P. Liu, Z. Chen, J. Liu, L. Shen, X. Zhang, J. Cui, T. Li, Y. Cui, Y. Ren, Micromachines **13**, 846 (2022).
[14] P. Mukherjee, S. Banerjee, S. Pahadsingh, W. Bhowmik, B. Appasani, Y. I. Abdulkarim, J. Optoelectron. Adv. M. **25**(3-4), 128 (2023).
[15] A. N. Razani, P. Rezaei, P. Zamzam, S. A. Khatami, O. M. Daraei, Optics Communications **524**, 128775 (2022).
[16] P. Mukherjee, S. Basu, P. Dutta, S. Banerjee, A. V. Jha, B. Appasani, Y. Abdulkarim, Metamaterials for Microwave and Terahertz Applications, Nova Science Publishers: New York, USA, Ch. 9, 191 (2022).
[17] P. Zamzam, P. Rezaei, Y. I. Abdulkarim, O. M. Daraei, Optics and Laser Technology **163**(25), 109444 (2023).
[18] A. N. Razani, P. Rezaei, Micro and Nanostructures **163**, 107153 (2022).
[19] S. Banerjee, U. Nath, Shruti, A. V. Jha, S. Pahadsingh, B. Appasani, N. Bizon, A. Srinivasulu, 13th International Conference on Electronics, Computers and Artificial Intelligence (ECAI), 1 (2021).
[20] S. Banerjee, U. Nath, P. Dutta, A. V. Jha, B. Appasani, N. Bizon, Inventions **6**, 78 (2021).
[21] M. R. Nickpay, M. Danaie, A. Shahzadi, Plasmonics **17**, 237 (2022).
[22] A. S. Saadeldin, M. F. Hameed, E. M. Elkaramany, S. Obayya, IEEE Sensors Journal **19**, 7993 (2019).
[23] S. Banerjee, P. Dutta, S. Basu, S. K. Mishra, B. Appasani, S. Nanda, Y. I. Abdulkarim, F. F. Muhammadsharif, J. Dong, A. V. Jha, N. Bizon, P. Thounthong, Symmetry **15**(1), 24 (2023).
[24] B. Li, Y. Liang, X. Xu, X. Xu, J. Chen, Y.-S. Lin, Physica E: Low-dimensional Systems and Nanostructures **151**, 115740 (2023).
[25] Y. Cheng, Y. Qian, H. Luo, F. Chen, Z. Cheng, Physica E: Low-dimensional Systems and Nanostructures **146**, 115527 (2023).
[26] J. Jiang, Z. Yang, W. Xu, H. Zhou, Y. Wu, H. Zhu, X. Zhang, B.-X. Wang, Modern Physics Letters B **37**, 2350097 (2023)
[27] W. Guo, L. Zhai, Z. M. El-Bahy, Z. Lu, L. Li, A. Y. Elnaggar, M. M. Ibrahim, H. Cao, J. Lin, B. Wang, Advanced Composites and Hybrid Materials **6**(3), 92 (2023).

*Corresponding author: bhargav.appasanifet@kiit.ac.in